Generation and Optimization of Laguerre-Gaussian Modes Using a Spatial Light Modulator: A Simulation Approach

Celina Kunert

Bachelorarbeit in Physik
angefertigt im Institut für Angewandte Physik

vorgelegt der
Mathematisch-Naturwissenschaftlichen Fakultät
der
Rheinischen Friedrich-Wilhelms-Universität
Bonn

September 2024

Contents

CHAPTER 1

Introduction

In recent years, vortex beams carrying orbital angular momentum (OAM) have gained significant attention due to their unique phase characteristics, including a helical wavefront, a central intensity null, and a phase singularity. These features make OAM beams promising for various applications, such as optical communication, rotational sensing, and particle manipulation. Consequently, researching the generation and application of OAM beams is crucial for advancing experimental techniques and broadening their use in practical settings.[1]

Light beams with OAM provide intriguing opportunities for studying the conservation of angular momentum in light-matter interactions. When light carrying OAM interacts with atoms, the question arises of how the atom's quantized angular momentum—comprising intrinsic spin, spatial OAM, and mechanical rotation—responds. This interaction helps to probe the quantum properties of light's OAM, enhancing our fundamental understanding of light-matter dynamics and enabling the development of OAM-based applications such as quantum memories, frequency converters, and advanced sensors.[2]

The Rubidium Quantum Optics (RQO) project at the University of Bonn explores the manipulation of single photons using a quantum-nonlinear medium composed of ultracold Rydberg atoms. Rydberg quantum optics utilizes the strong interactions between Rydberg atoms to create a nonlinear medium that can influence otherwise non-interacting photons.[3] In the current RQO experiment, rubidium atoms are laser-cooled and trapped in a magneto-optical trap (MOT) and then in a large dipole trap, cooling the atomic cloud to temperatures below 4 K. The aim is to create Rydberg superatoms—ensembles of atoms that can collectively share a single excitation within the Rydberg blockade radius.[4] Future experiments will investigate how Rydberg-mediated interactions between photons in the ultracold gas alter the outgoing light mode. Currently, the setup uses Gaussian modes, but plans include probing and collecting light in different OAM modes to observe the influence of Rydberg interactions and to explore the potential of probing atoms with OAM beams.

To achieve these experimental goals, Spatial Light Modulators (SLMs) are crucial for generating and detecting LG modes, allowing precise control over the phase and amplitude of light beams[5] SLMs are useful for preparing the probe light in specific OAM states and collecting the resulting light after interactions with the Rydberg atoms. Their ability to dynamically modify the phase and amplitude of light makes SLMs invaluable tools for this research.

This thesis supports these plans by focusing on the theoretical and experimental generation of Laguerre-Gaussian (LG) modes. Chapter 2 lays the theoretical groundwork for computer-generated holograms (CGHs) and Fourier optics, detailing the calculation methods for phase-only and amplitude-modulated holograms, and explaining the integration of SLMs in optical systems. Chapter 3 presents the numerical simulations of LG modes using these methods, evaluating their effectiveness in reproducing theoretical results and comparing the different approaches. Chapter 4 details the experimental setup used to generate LG modes, highlighting the adjustments made to optimize the system for accurate mode production. Finally, the thesis concludes with a summary of the findings and their implications for future OAM-based experiments within the RQO project.

By integrating advanced SLM techniques with precise experimental setups, this work contributes to the broader goals of the RQO project, enhancing the understanding of light-matter interactions and paving the way for novel OAM-based quantum applications.

CHAPTER 2

Theoretical Foundations of CGHs and Fourier Optics

Computer-Generated Holograms (CGHs) have become a key tool in the generation and manipulation of complex optical beams, including those with optical vortices (OV) and Laguerre-Gaussian (LG) modes. These beams, characterized by unique wavefront singularities, regions of zero intensity, and orbital angular momentum, have garnered significant attention due to their potential in both fundamental physics and practical applications such as optical trapping, precise measurement, and information processing. Among the various techniques available for generating OV beams, the holographic approach is particularly efficient, leveraging interference patterns to shape incident light into desired modes. This section delves into the theoretical underpinnings of CGHs tailored for Laguerre-Gaussian modes, focusing on phase and amplitude modulation principles and the foundational aspects of Fourier optics that guide their design and implementation.[6]
For further information about the beam profiles of Laguerre-Gaussian modes and the principles and operations of Spatial Light Modulators (SLMs), the reader is advised to consult the Bachelor thesis of Kimberly Kurzbach [7], where these topics are explained in detail.

2.1 Calculation of Computer-Generated Holograms for Laguerre-Gaussian Modes

In the following sections, we will discuss different approaches to calculating holograms for LG modes. First, we explore phase-only holograms, which manipulate only the phase of the light to generate the desired modes. Next, we examine amplitude-modulated holograms, which involve both phase and amplitude modulation. For these, two methods are presented: an exact approach that provides high fidelity in mode generation and a simplified approach that balances performance and computational complexity.

2.1.1 Phase-Only Holograms

To generate LG beams, it is necessary to determine the phase patterns based on the electric field amplitude of the desired LG beam under the paraxial and scalar wave approximations. Assuming the

LG beam propagates in the z-direction and is focused at z = 0, the electric field amplitude $u_l^p(r, \theta, z)$ is given by

$$u_l^p(r,\theta,z) = (-1)^p \sqrt{\frac{2}{\pi}\frac{p!}{(p+|l|)!}} \frac{\left(\sqrt{2}\frac{r}{w_z}\right)^{|l|}}{w_z} \exp\left(-\frac{r}{w_z}\right)^2 L_p^{|l|}\left(\frac{2r^2}{w_z^2}\right) \times \exp(-il\theta) \exp\left(-i\frac{r^2}{w_z^2} z/z_R\right) \exp\left(i\,(2p+|l|+1)\tan^{-1}\left(z/z_R\right)\right) \tag{2.1}$$

where $L_p^(|l|)(x)$ is a generalized Laguerre polynomial and z_R and $w_z = \sqrt{z^2 + z_R^2}/(kz_R)$ represent the Rayleigh length and beam radius at position z, respectively. k is the wavenumber of the incident light. [8]

The phase structure of the LG beam is characterized by the azimuthal term $\exp(-il\theta)$ and $L_p^{|l|}\left(\frac{2r^2}{w_z^2}\right)$. Given that the Laguerre polynomial $L_p^(|l|)(x)$ changes its sign at each x_i, this results in a helical phase pattern $\Phi_L(r, \phi)$ characterized by phase discontinuities at each r_i. This pattern is used to generate the LG_p^l beam by modulating an incident plane wave. The phase modulation can be expressed as

$$\Phi_L(r,\phi) = -l\phi + \pi\theta\left(-L_p^{|l|}\left(\frac{2r^2}{w_0^2}\right)\right) \tag{2.2}$$

where $\theta(x)$ represents the unit step function. In use with an SLM, the phase pattern is constricted to the interval 0 and 2π. [9].

However, Output beams from the LCOS-SLM often contain unmodulated components that negatively impact beam quality. To separate these unwanted parts from the desired beam, a blazed phase grating pattern $\Phi_g(x, y)$ of the form

$$\Phi_g(x,y) = \mathrm{Mod}\left(\frac{2\pi x}{\Lambda}, 2\pi\right) \tag{2.3}$$

is added to the phase structure where Λ is the grating period, which optimizes how efficiently the light is diffracted.[5]

In combination of the phase pattern $\Phi_L(r, \phi)$ and the blazed phase grating pattern $\Phi_g(x, y)$ holograms like Image 1 can be obtained.

2.1.2 Amplitude Modulated Holograms

To accurately generate arbitrary beams, it's essential to control both the phase and amplitude of the light. Thus we will now examine the approaches presented by Bolduc et al.[10], which demonstrate effective methods for achieving this simultaneous control.

Exact Calculation Method

To encode both amplitude and phase on a phase-only hologram, we define the desired output field as

$$E(\mathbf{r}_\perp; z_0) = A(\mathbf{r}_\perp, z_0) e^{i\Phi(\mathbf{r}_\perp, z_0)}, \tag{2.4}$$

where A represents the amplitude and Φ is the phase at a given plane. This approach allows us to control the light's behavior by adjusting its shape and wavefront.
The imprinted phase profile on the hologram is expressed as

$$\Psi(m, n) = M(m, n)\text{Mod}(F(m, n) + 2\pi m/\Lambda, 2\pi), \tag{2.5}$$

where M modulates the amplitude, F defines the phase information of the desired optical field and m and n are the pixel coordinates. Analogous to Section 2.1.1 Λ represents the grating period. In this case, to generate LG modes, F is equal to Φ_L as defined in Equation 2.2.
Once the incident plane wave passes through the hologram, it acquires the encoded phase pattern and a spatial filter is then used to isolate the first diffraction order, allowing only the desired optical field components to propagate. The resulting field can be expressed as

$$T_1(m, n) = -\text{sinc}(\pi M - \pi) e^{i(F - \pi M)}. \tag{2.6}$$

This shows shows that the phase πM introduced by amplitude modulation is corrected by subtracting it in the encoded phase function F.
To ensure that the output field matches the desired target field exactly, the functions M and F are set to

$$M = 1 - \frac{1}{\pi}\text{sinc}^{-1}(A), \quad \text{and} \quad F = \Phi - \pi M. \tag{2.7}$$

This exact modulation method allows independent control of the amplitude and phase, ensuring high fidelity in the generation of complex optical modes.
While the exact method involving the inverse sinc function provides precise control over amplitude and phase, it poses significant practical challenges as calculating the inverse sinc function for each pixel on the hologram is computationally intensive and time-consuming. This complexity can make the approach impractical when working with high-resolution holograms or when quick results are essential.

Simplified Calculation Method

To address these limitations, a more straightforward and computationally efficient approach can be employed, which avoids the heavy calculations required by the exact method. This simplified technique builds on the earlier work of Davis et al.[11], where the modulation functions are set as $M = A$ and $F = \Phi$. In this scheme, the optical field after passing through the spatial filter is approximately described by:

$$\operatorname{sinc}(\pi A - 1) \exp\left(i(\Phi + \pi A)\right). \tag{2.8}$$

Although this method does not perfectly reproduce the desired amplitude, it still provides a generated amplitude profile that closely resembles the target. The deviation between the generated and desired amplitudes is minor, with the maximum difference being less than 0.161:

$$|\operatorname{sinc}(\pi A - 1) - A| < 0.161. \tag{2.9}$$

This level of discrepancy is often acceptable, especially when compared to the more problematic alteration in the phase profile caused by the additional term πA.

To address the extra phase term introduced in the simplified method proposed, a refinement of the phase encoding function can be implemented:

$$F = \Phi - \pi A. \tag{2.10}$$

This adjustment reduces the unwanted phase shift that often affects the beam's overall quality more significantly than amplitude discrepancies. Although this refinement does not fully correct the amplitude deviation, it significantly improves the accuracy of the generated phase profile, aligning it closer to the desired optical field. The approach provides a straightforward and efficient solution when exact replication of the optical field is not required, balancing computational simplicity with enhanced fidelity.

2.2 Fourier Optics Principles

Fourier Optics provides a foundational understanding of light propagation through optical systems, focusing on how wavefronts are transformed by lenses, apertures, and other elements. By applying Fourier transforms, this approach offers essential insights into diffraction and interference phenomena, forming the basis for the simulations and analyses carried out in this work. This section begins by examining the fundamental theory of diffraction, followed by the integration of Spatial Light Modulators in optical systems, and concludes with the application of Discrete Fourier Transform for intensity calculations.

2.2.1 Diffraction Phenomena in Fourier Optics

The diffraction of light through apertures can be described using the scalar theory of diffraction, particularly relevant for small angles and homogeneous liquid crystal modulators like the SLM. The Helmholtz equation, derived from the wave equation, serves as the foundation for analyzing light propagation and can be expressed as:

$$(\nabla^2 + k^2)U(\mathbf{r}) = 0, \tag{2.11}$$

where $k = \frac{2\pi}{\lambda}$ is the wave number, and $U(\mathbf{r})$ represents the complex amplitude of the light wave.

This equation is essential for understanding how light behaves under different conditions, especially when passing through optical elements like lenses and apertures.[12]

Huygens-Fresnel Principle

The Huygens-Fresnel principle explains wave propagation by treating each point on a wavefront as a source of secondary spherical wavelets. These wavelets constructively and destructively interfere to form the resultant wavefront, providing a qualitative explanation of reflection, refraction, and diffraction.[13]

To quantitatively describe diffraction, Fresnel refined the principle by introducing wave coherence, phase considerations, and an obliquity factor $\psi(\theta)$, accounting for directional effects. This adjustment allows the complex amplitude at an observation point to be modeled as a superposition of contributions from all points on the wavefront.

$$U(P_O) = \frac{1}{i\lambda} \iint_S U(P_A) \frac{e^{ikr_{OA}}}{r_{OA}} \psi(\theta)\, ds, \tag{2.12}$$

where r_{OA} is the distance from the aperture point P_A to the observation point P_O. This equation serves as the mathematical foundation for diffraction analysis.[14]

Fresnel and Fraunhofer Approximations

The Fresnel approximation simplifies the general diffraction integral by assuming small diffraction angles (paraxial approximation). By approximating the distance term r_{OA} and factoring out exponential terms, the Fresnel diffraction integral becomes

$$U(x,y) = e^{ikz} \frac{e^{i\frac{k}{2z}(x^2+y^2)}}{i\lambda z} \iint_{-\infty}^{\infty} U(\xi,\eta) e^{i\frac{k}{2z}(\xi^2+\eta^2)} e^{-i\frac{2\pi}{\lambda z}(x\xi+y\eta)}\, d\xi d\eta. \tag{2.13}$$

This integral is effectively a Fourier transform evaluated at spatial frequencies $f_x = \frac{x}{\lambda z}$ and $f_y = \frac{y}{\lambda z}$, describing the wave field near the aperture (near-field or Fresnel region).

When the observation point is far enough from the aperture (satisfying the condition $z \gg \frac{k(\xi^2+\eta^2)_{\max}}{2}$), the Fraunhofer approximation applies, further simplifying the expression to:[12]

$$U(x,y) = e^{ikz} \frac{e^{i\frac{k}{2z}(x^2+y^2)}}{i\lambda z} \iint_{-\infty}^{\infty} U(\xi,\eta) e^{-i\frac{2\pi}{\lambda z}(x\xi+y\eta)}\, d\xi d\eta. \tag{2.14}$$

Fresnel Approximation in Simulations

The validity of the Fresnel approximation is determined by the Fresnel number:

$$N_F = \frac{D^2}{\lambda L}, \tag{2.15}$$

where D is the aperture size, λ is the wavelength, and L is the distance to the observation point. For $N_F \geq 1$, the Fresnel approximation holds, which is the case in our experimental setup. This approximation is suitable for simulations as it captures the essential diffraction behavior without the need for the more complex far-field assumptions.[12]

2.2.2 SLM Integration in Optical Systems

Liquid Crystal on Silicon Spatial Light Modulators (LCOS-SLM) are devices that modulate light by altering the phase of an incoming beam. They consist of a layer of birefringent liquid crystals atop a reflective surface, divided into an array of pixels. Each pixel's refractive index is controlled by an applied voltage, allowing the phase shift across the surface to vary between 0 and 2π. The SLM used in this thesis has 792×600 pixels, each measuring $12.5\,\mu m$ on a side.[15]

When a phase hologram is displayed on the SLM, it modulates the incoming light such that the desired image is formed in the focal plane of a lens placed behind the SLM. The formation of this image involves the optical transformation properties of the lens, which acts as a Fourier transformer, converting the modulated light into a specific intensity pattern at the focal plane. This transformation is essential for understanding the light distribution and intensity resulting from the applied phase holograms.[12]

A key aspect of this optical setup is the lens's ability to perform a two-dimensional Fourier transform, which is integral to the generation of the desired intensity pattern. The lens, in conjunction with the SLM, transforms the modulated light into a specific image at its focal plane. The wave field before and after the lens, as well as at the focal plane, are represented as $U_{\text{lens}}(u,v)$, $U'_{\text{lens}}(u,v)$, and $U_f(x,y)$, respectively. Using the Fresnel approximation, the complex field amplitude $U_f(x,y)$ at the lens's focal plane can be described in three steps [12]:

1. **Fresnel Diffraction Integral:** The relationship between the field after the lens and the field in the focal plane is given by the Fresnel diffraction integral:

$$U_f(x,y) = \frac{e^{ikz}}{i\lambda f} e^{i\frac{k}{2f}(x^2+y^2)} \iint_{-\infty}^{\infty} U'_{\text{lens}}(u,v) e^{i\frac{k}{2f}(u^2+v^2)} e^{-i\frac{2\pi}{\lambda f}(xu+yv)}\, dudv. \tag{2.16}$$

2. **Lens Transformation Function:** The transmission through the lens modifies the field as:

$$U'_{\text{lens}}(u,v) = e^{-i\frac{k}{2f}(u^2+v^2)} U_{\text{lens}}(u,v), \tag{2.17}$$

   which simplifies the diffraction integral to a Fourier transform:

$$U_f(x,y) = \frac{e^{ikf}}{i\lambda f} e^{i\frac{k}{2f}(x^2+y^2)} \text{FT}\{U_{\text{lens}}(u,v)\}(f_x, f_y), \tag{2.18}$$

   where $f_x = x/\lambda f$ and $f_y = y/\lambda f$.

3. **Free Space Propagation:** The propagation of the wave field from the SLM to the lens can be expressed in terms of Fourier transforms [12]:

$$\text{FT}\{U_{\text{lens}}(f_x, f_y)\} = e^{-i\pi\lambda d(f_x^2+f_y^2)} \text{FT}\{U_{\text{SLM}}(f_x, f_y)\}, \tag{2.19}$$

   with the distance d and the corresponding phase shift due to free-space propagation.

Combining these relations, the complete propagation from the SLM to the focal plane is given by

$$U(x,y) = \frac{e^{i\frac{k}{2f}(1-\frac{d}{f})(x^2+y^2)}}{i\lambda f} \iint_{-\infty}^{\infty} U_{\text{SLM}}(\xi,\eta) e^{-i\frac{2\pi}{\lambda f}(x\xi+y\eta)}\, d\xi d\eta. \tag{2.20}$$

$$= \frac{e^{i\frac{k}{2f}(1-\frac{d}{f})(x^2+y^2)}}{i\lambda f} \text{FT}\{U_{\text{SLM}}(f_x, f_y)\} \tag{2.21}$$

The intensity $I(x, y)$ of the electromagnetic field at the focal plane, which is of primary interest in this setup, is then proportional to the squared magnitude of the Fourier transform of the SLM's output:

$$I(x,y) = |U_f(x,y)|^2 \propto \left|\text{FT}\{U_{\text{SLM}}(\xi,\eta)\}\right|^2_{f_x=x/\lambda f,\, f_y=y/\lambda f}, \tag{2.22}$$

highlighting the lens's role as a Fourier lens, effectively producing an image of the far-field diffraction pattern.[16]

2.2.3 Intensity Computation Using Discrete Fourier Transform

Building on the principles of light modulation and Fourier transformation introduced in the previous section, this part delves into the specific calculation of intensity patterns produced by the SLM. When the SLM displays a phase hologram, it modulates the incoming light, and the resulting wave field at the focal plane of a lens is determined by a series of transformations that can be effectively described using the Discrete Fourier Transform (DFT).

The optical field generated by the SLM, denoted as U_{SLM}, consists of the incoming Gaussian beam U_{in}, the phase modulation $e^{i\phi_{(n,m)}}$, and the pixelated aperture function of the SLM. This can be mathematically expressed as[17]:

$$U_{\text{SLM}} = U_{\text{in}} \cdot e^{i\phi_{(n,m)}} \cdot \text{rect}\left(\frac{x}{\Delta x} - n - \frac{N_x - 1}{2}\right) \cdot \text{rect}\left(\frac{y}{\Delta y} - m - \frac{N_y - 1}{2}\right),$$

where:

- Δx and Δy are the pixel sizes.
- N_x and N_y are the number of pixels in the x and y directions.
- n and m are indices corresponding to the pixel positions.

The Fourier transform of the rectangular aperture functions results in sinc functions, with spatial shifts inducing corresponding phase shifts in the frequency domain:

$$\text{FT}\left[\text{rect}\left(\frac{x}{\Delta x} - n - \frac{N_x - 1}{2}\right)\right] = \Delta x \cdot \text{sinc}(\Delta x \cdot f_x) \cdot e^{-i2\pi f_x (n+\frac{N_x}{2})\Delta x}.$$

Combining these transforms with the phase modulation of the SLM, the total Fourier transform of U_{SLM} is:

$$\mathrm{FT}\{U_{\mathrm{SLM}}\} = \Delta x \Delta y \cdot \mathrm{sinc}(\Delta x \cdot f_x) \cdot \mathrm{sinc}(\Delta y \cdot f_y) \cdot e^{-i\pi(f_x N_x \Delta x + f_y N_y \Delta y)} \cdot \mathrm{DFT}[e^{i\phi}] \left(\frac{x}{L_x N_x}, \frac{y}{L_y N_y} \right),$$

where the DFT of the phase modulation term is:

$$\mathrm{DFT}[A](k,l) = \sum_{m=0}^{M-1} \sum_{n=0}^{N-1} A(m,n) e^{-i2\pi\left(\frac{km}{M} + \frac{ln}{N}\right)}.$$

This expression emphasizes the interplay between the phase modulation of the SLM and the system's optical properties, shaping the observed intensity pattern at the lens's focal plane. The pixelated structure of the SLM, combined with the Fourier transforming capabilities of the lens, enables fine control over the light distribution, underscoring the effectiveness of Fourier optics in manipulating optical fields and tailoring beam shapes.[12]

CHAPTER 3

Numerical Simulations of Laguerre-Gaussian Mode Generation

This chapter outlines the numerical simulations conducted to model the generation of Laguerre-Gaussian modes using various phase and amplitude modulation methods. The simulations were performed using Python and focused on replicating the theoretical predictions of beam shaping with phase-only and amplitude-modulated holograms. Detailed descriptions of the simulation setup, the algorithms used, and the resulting beam profiles are provided. These simulations serve as a critical step in validating the experimental results and understanding the effectiveness of different hologram calculation methods.

3.1 Implementation of Simulation Methods in Python

The numerical simulations of Laguerre-Gaussian (LG) modes were implemented using Python, utilizing libraries such as NumPy for numerical operations, SciPy for special functions and optimization, and Matplotlib for visualizing results. The primary objective was to simulate the generation of LG modes using various phase mask calculation methods, as outlined in the theoretical section.

Simulation Approach:

1. **Beam Initialization and Grid Setup:** The simulation begins by defining the spatial grid for the incoming Gaussian beam and the phase masks. The beam is initialized with parameters such as beam waist and wavelength, and the simulation grid is set up to match the resolution of the SLM (792×600 pixels).
2. **Phase and Amplitude Modulation Methods:** Three modulation methods were implemented: Phase-Only, Exact Amplitude Modulation, and Simplified Amplitude Modulation, each corresponding to the theoretical methods discussed in Section 2.1. The Phase-Only method alters only the phase, while the Exact and Simplified methods modulate both phase and amplitude, with the latter offering a computationally simpler approximation.
3. **Fourier Transform and Fresnel Diffraction:** The modulated beam undergoes a Discrete Fourier Transform (DFT) to simulate its propagation through the optical system, utilizing the

Fresnel approximation as outlined in Section 2.2.3. The DFT accounts for the pixelated nature of the SLM, applying sinc functions to model the diffraction effects caused by the pixel grid.

4. **Intensity Calculation:** The intensity patterns of the resulting beam are computed from the complex amplitude distributions in the focal plane of a lens, which acts as a Fourier transformer. These patterns are compared with theoretical expectations to evaluate the quality of the generated LG modes.

5. **Visualization and Analysis:** The results are visualized by plotting the intensity patterns and comparing them against theoretical Laguerre-Gaussian distributions. This includes identifying and analyzing diffraction peaks to ensure accurate mode generation.

The code's structure reflects the complexity of each modulation method, with the exact amplitude modulation providing the highest fidelity at the cost of computational intensity. Further analysis of the simulation results, including mode fitting and waist measurements, provides insights into the performance and accuracy of these approaches.

3.2 Results from Laguerre-Gaussian Mode Simulations

This section presents the results obtained from the numerical simulations of Laguerre-Gaussian mode generation using the three different phase mask calculation methods: Phase-Only, Exact Amplitude Modulation, and Simplified Amplitude Modulation. Each method's simulated intensity patterns and the corresponding analyses are discussed, highlighting the differences in mode purity, alignment with theoretical expectations, and computational efficiency. These results provide a detailed assessment of how each method performs in replicating the desired optical fields, emphasizing their strengths and limitations.

3.2.1 Phase-Only Method

The Phase-Only Method was evaluated for its ability to generate higher-order Laguerre-Gaussian (LG) modes using an SLM. This method focuses on applying a phase modulation to the incoming Gaussian beam while keeping the amplitude modulation minimal, aiming to replicate the desired LG modes effectively.

Waist Ratio Optimization

To determine the optimal waist ratio between the incoming Gaussian beam (w_0) and the waist parameter (w) used for calculating the phase hologram, different ratios were tested. As shown in Figure 3.1, the best results were achieved with a ratio of $w/w_0 = 0.45$, yielding the highest mean R^2 value of approximately 0.68. The plot indicates that the waist ratio significantly impacts the fidelity of the generated modes, with deviations leading to poorer quality reconstructions.

Generated Modes

The LG modes generated with the optimized parameters ($w_0 = 40$, $w = 18$) are displayed in Figure 3.2. The simulations show varying success across different modes; some modes closely resemble the

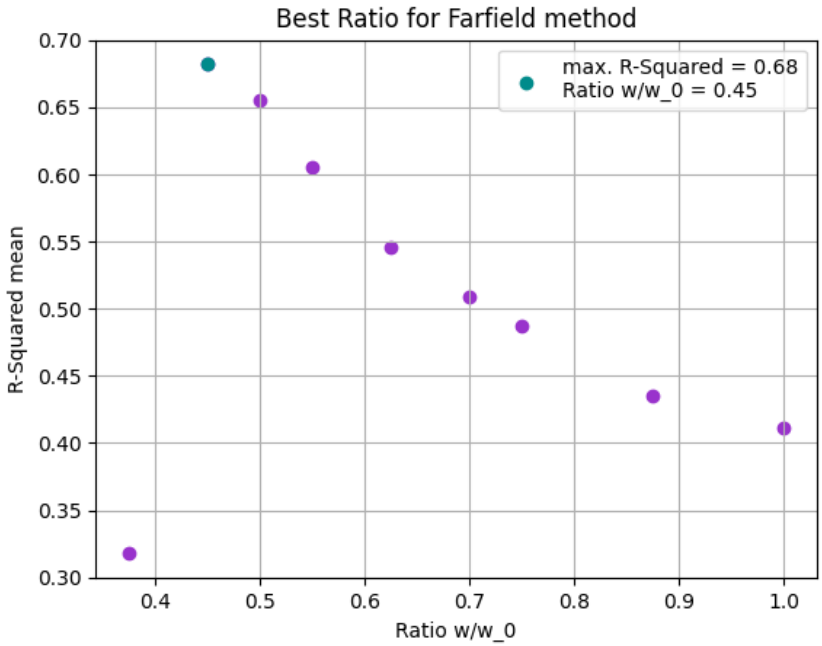

Figure 3.1: R^2 Values for Different Phasemask Waists - Phase-Only Mode. The optimal waist of 45 pixels corresponds to a ratio of approximately 0.68, which differs from the simulation results.

theoretical expectations, while others display considerable deviations. This variability highlights that the Phase-Only Method's performance is highly mode-dependent, particularly for higher-order modes.

Fitted Waist Analysis

Figure 3.3 presents the fitted waist values in the x- and y-directions for each generated mode, demonstrating consistency in waist measurements across both axes. However, slight variations were observed between modes, with a mean waist of approximately 7.00×10^{-8} m and minimal variance ($\sim 1.19 \times 10^{-16}$). These findings suggest that the generated beam shapes are reasonably symmetrical, aligning well with the expected characteristics of LG modes.

R^2 Value Distribution

The distribution of R^2 values across different modes, as depicted in Figure 3.4, shows significant variability, echoing the observations made from the visual mode generation results. With an average R^2 value of 0.68, the method demonstrates moderate success, though mode-specific performance varies significantly.

Mode Purity Analysis

To better understand the method's limitations, mode purities were assessed by comparing R^2 values for different LG modes across various waist ratios (Figures 3.5 and 3.6). The results reveal a consistent

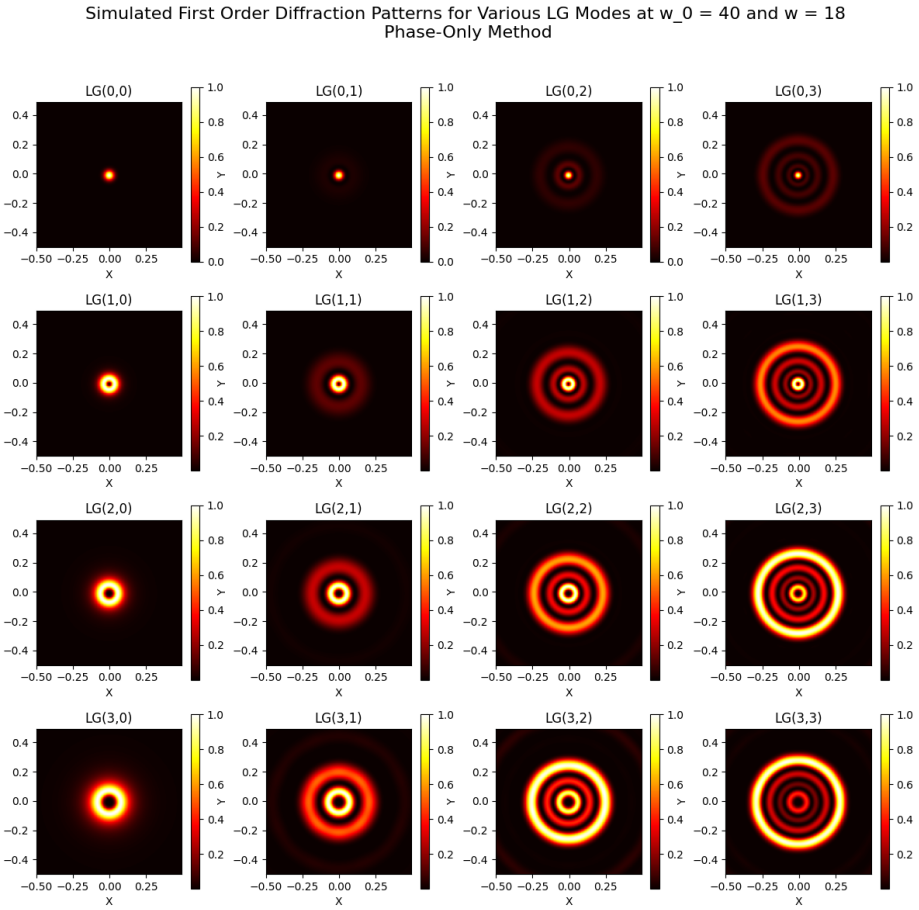

Figure 3.2: Simulated First Order Diffraction Patterns for Various LG Modes using Phase-Only Method.

pattern across modes, with optimal waist ratios differing slightly between modes, indicating that each mode requires specific tuning for best results.

Overall, the Phase-Only Method proved effective for generating LG modes, though its success is highly sensitive to both the mode parameters and the choice of waist ratio. Further adjustments and optimizations, particularly in mode-specific settings, could enhance the method's performance.

3.2.2 Comparison of Amplitude Modulation Methods

The performance of the exact and simplified amplitude modulation methods was evaluated using simulations, focusing on the fidelity of generated Laguerre-Gaussian (LG) modes. The primary goal was to determine the optimal waist ratio w/w_0 that maximizes the mode purity, characterized by the R^2 values.

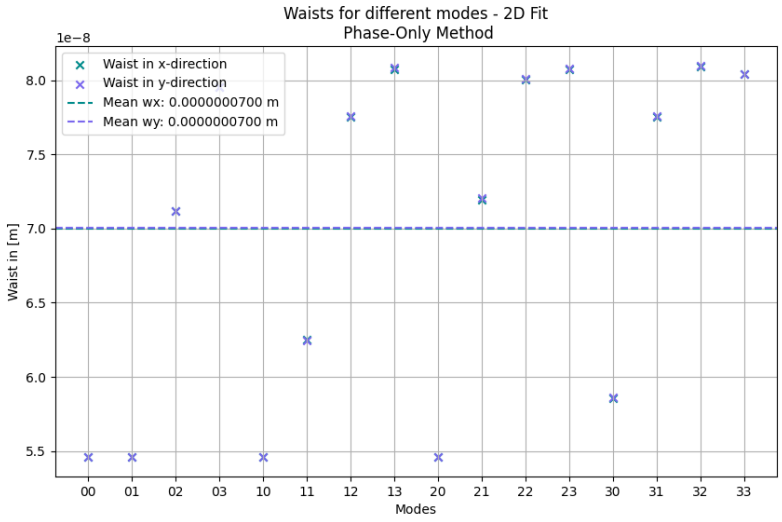

Figure 3.3: Waist Simulations for Different LG Modes - Phase-Only Method.

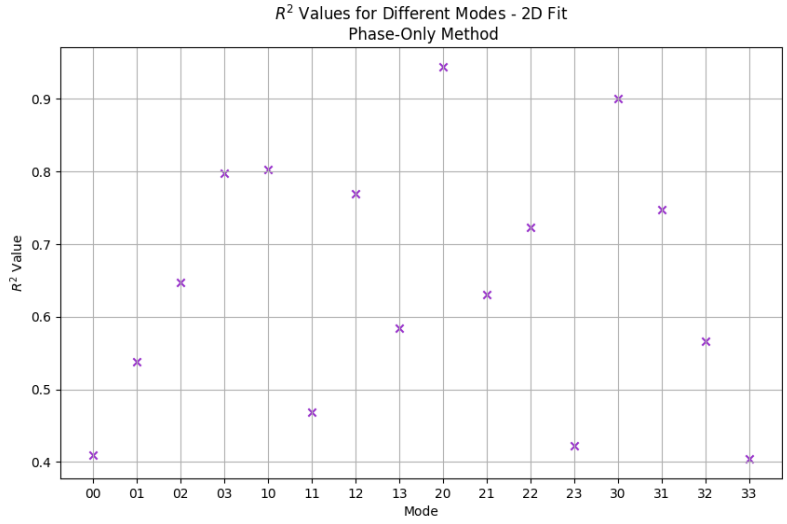

Figure 3.4: R^2 Values for Different Simulated Modes - Phase-Only Method. The average .

Optimized Waist Ratio

Figure 3.7 shows the mean R^2 values for different waist ratios for both the exact and simplified methods. The best mean R^2 is observed at a waist ratio of approximately 0.1, corresponding to $w_0 = 280$ pixels and $w = 30$ pixels. It is noteworthy that the mean R^2 values for both methods remain significantly higher compared to the phase-only method, with values approaching 1. However, for larger waist ratios, the R^2 values decrease, which may be attributed to the resolution limits in the Fourier plane as the effective image size decreases with increasing w.

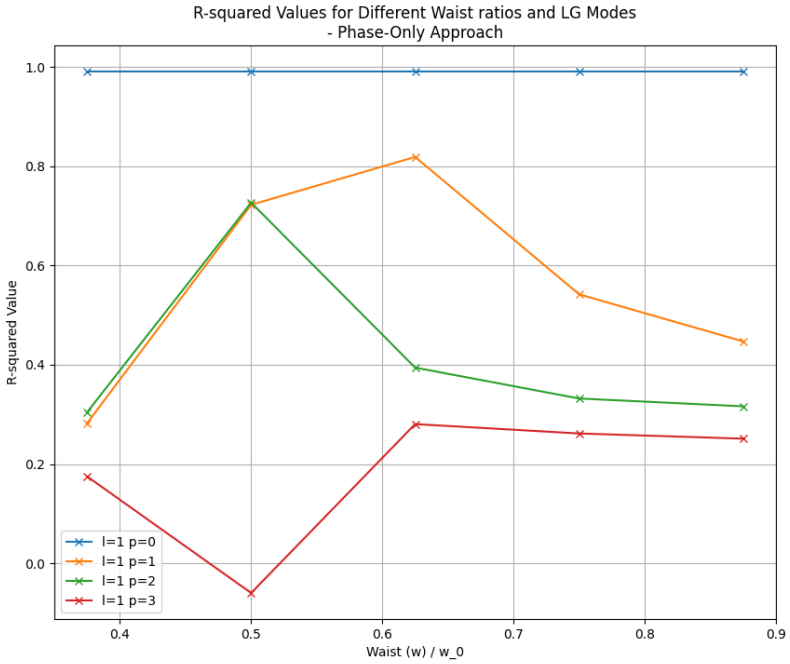

Figure 3.5: Mode Purity for Different l Values - Phase-Only Method. Variations in the optimal waist ratio for different modes are observed.

Simulation of All LG Modes

The optimized parameters were used to generate all LG modes, as shown in Figure 3.8 and Figure 3.9. Both methods successfully produce LG modes that closely resemble theoretical predictions, demonstrating high fidelity with minimal visual discrepancies.

Waist Fitting Analysis

Figures 3.10 and 3.11 present the fitted waist values in the x and y directions for the exact and simplified methods, respectively. The exact method shows a slightly better alignment between the x- and y-waists, with mean values of 4.7008×10^{-8} m (variance 2.517×10^{-20} m^2) and 4.7013×10^{-8} m (variance 4.144×10^{-20} m^2). The simplified method has mean values of 4.6864×10^{-8} m (variance 2.746×10^{-19} m^2) and 4.6929×10^{-8} m (variance 2.780×10^{-19} m^2), showing slightly higher variances but still maintaining overall good consistency.

R^2 Analysis of Individual Modes

Figures 3.12 and 3.13 display the R^2 values for each mode. Both methods yield R^2 values above 0.975 for all modes, with mean R^2 values of 0.9933 for the exact method and 0.9921 for the simplified method. These results confirm that the exact method only slightly outperforms the simplified method,

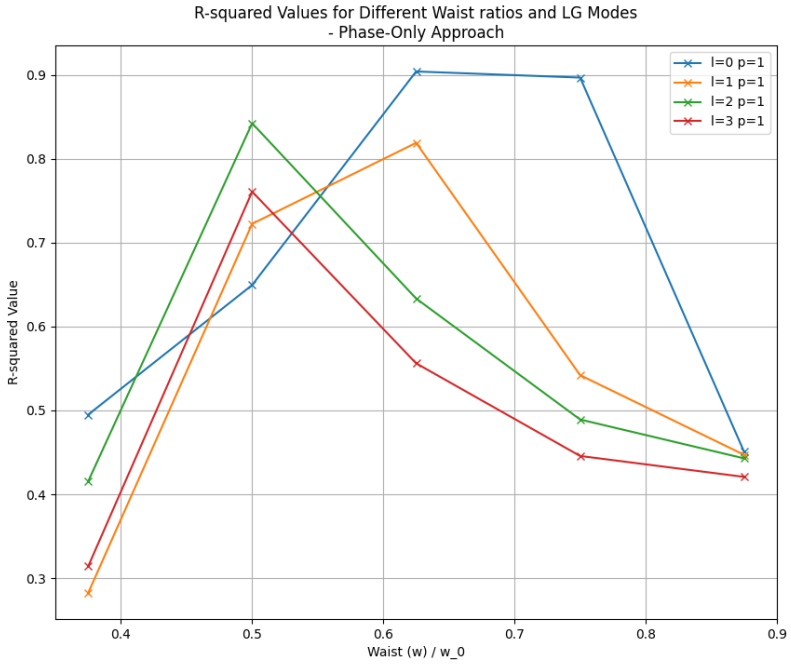

Figure 3.6: Mode Purity for Different p Values - Phase-Only Method.

emphasizing that the simplified approach provides almost equivalent fidelity with less computational effort.

Mode Purity Analysis

The mode purity, evaluated as the R^2 across various waist ratios and modes, reveals consistent patterns across both methods, as depicted in Figures 3.14 and 3.15. While both methods show the highest purity at the optimal waist ratio, the fidelity of the exact method declines more rapidly as the waist ratio increases, potentially due to the inherent limitations in the approximation of the inverse sinc function used in the exact method.

In conclusion, both the exact and simplified amplitude modulation methods provide high-quality LG modes, with the exact method showing slightly superior performance in terms of consistency and fidelity. However, the simplified method remains an efficient alternative with nearly comparable results, making it suitable for applications where computational simplicity is preferred.

3.3 Discussion and Limitations

The evaluation of the numerical simulations for generating Laguerre-Gaussian (LG) modes using different modulation techniques on Spatial Light Modulators (SLMs) highlighted several key findings and challenges. The three tested methods—phase-only modulation, exact amplitude modulation,

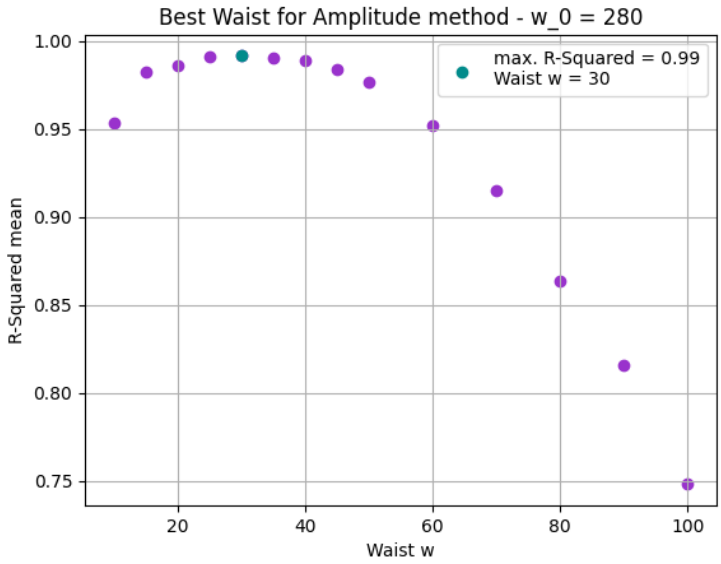

Figure 3.7: Mean R^2 values for different waist ratios. Optimal ratio found at $w_0 = 280$ and $w = 30$.

and simplified amplitude modulation—each showed varying levels of accuracy in reproducing the theoretical LG modes.

The amplitude modulation methods, both exact and simplified, showed significantly better performance compared to the phase-only modulation approach. The exact amplitude modulation method, in particular, achieved the highest R^2 values, indicating a closer match to the theoretical profiles. However, this method relies on more complex calculations, especially due to the inverse sinc approximation, which may introduce slight inaccuracies and increases computational demand. Despite these challenges, the exact method consistently showed a high degree of fidelity across all tested modes.

The simplified amplitude modulation method provided almost comparable results to the exact approach with a slightly lower mean R^2 value but maintained computational simplicity, making it an attractive alternative. However, minor discrepancies, especially for larger modes and higher waist ratios, were observed. This suggests that while the simplified method is practical, it may not fully capture the nuances required for precise mode generation at all conditions.

A notable limitation observed in all methods is related to the resolution constraints inherent in the numerical simulations. As the waist of the LG modes increases, the corresponding image in the Fourier plane becomes smaller, limiting the effective resolution and potentially degrading the R^2 values. Enhancing resolution could mitigate this issue but would require significantly more computational resources, which might not be feasible in real-time or resource-limited settings.

It is also important to acknowledge that these simulations were conducted under idealized conditions. Real-world imperfections, such as noise, optical aberrations, or SLM non-linearities, were not accounted for and could affect the actual performance of these methods. Additionally, the approximations used, especially in the exact amplitude method, represent a limitation in achieving truly "exact" results.

In conclusion, while the amplitude modulation methods provide a substantial improvement over

phase-only modulation in numerical simulations, each approach has its trade-offs. The exact method offers the highest accuracy at the cost of complexity, while the simplified method balances performance and practicality.

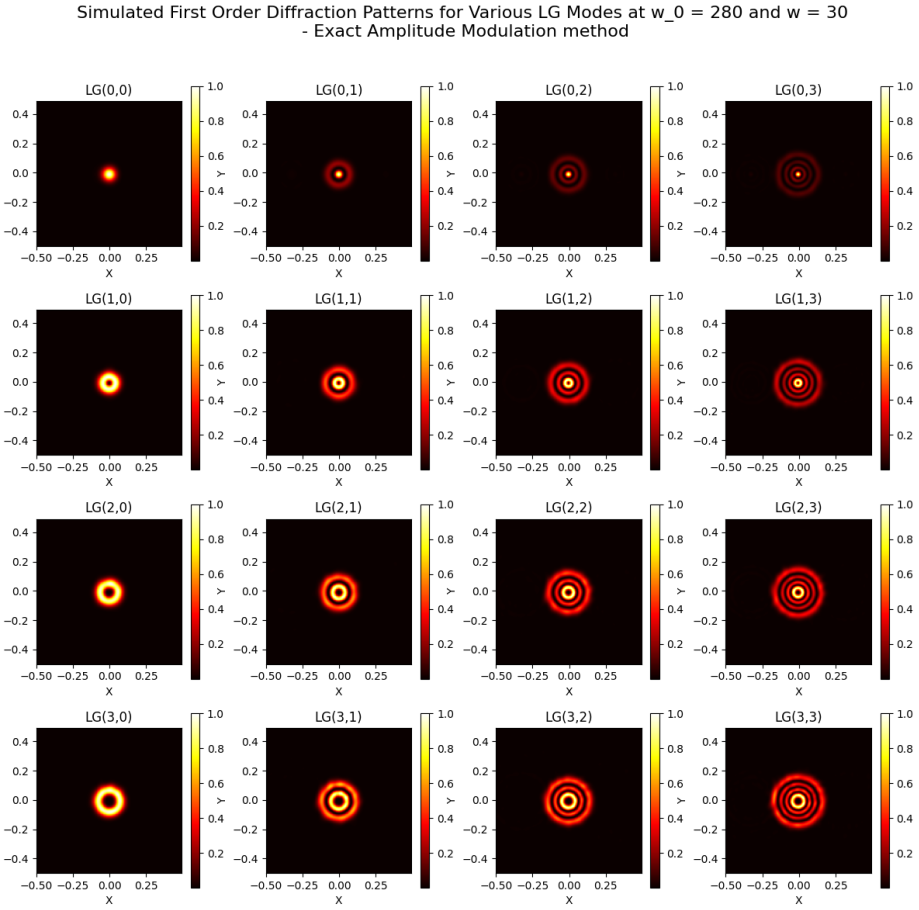

Figure 3.8: Simulated first-order diffraction patterns of various LG modes using the exact amplitude modulation method with optimized waist $w = 30$ pixels.

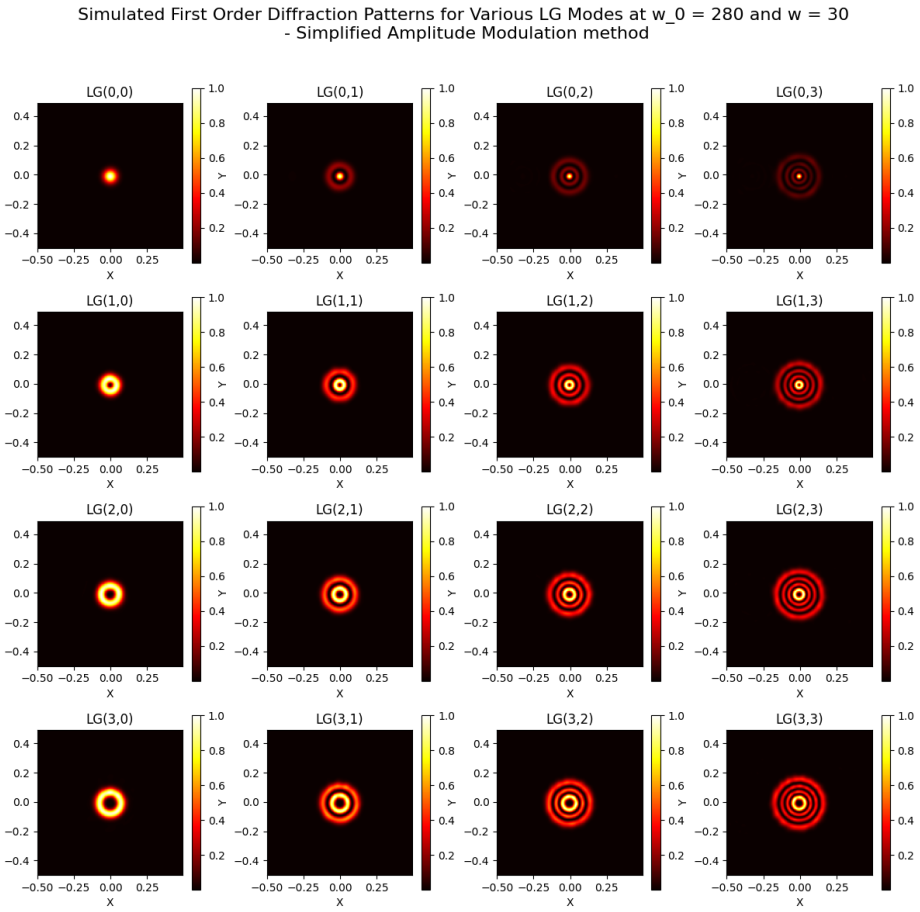

Figure 3.9: Simulated first-order diffraction patterns of various LG modes using the simplified amplitude modulation method with optimized waist $w = 30$ pixels.

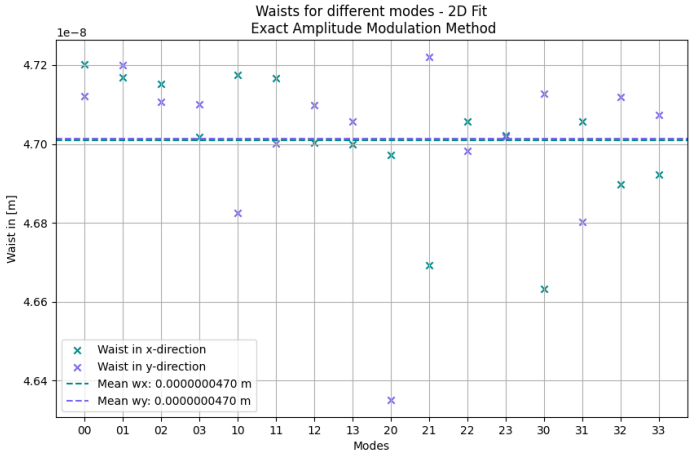

Figure 3.10: Fitted waists in x and y directions for the exact amplitude modulation method.

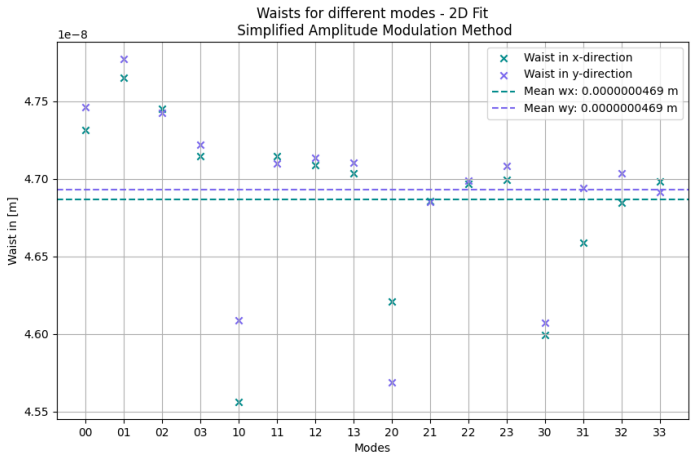

Figure 3.11: Fitted waists in x and y directions for the simplified amplitude modulation method.

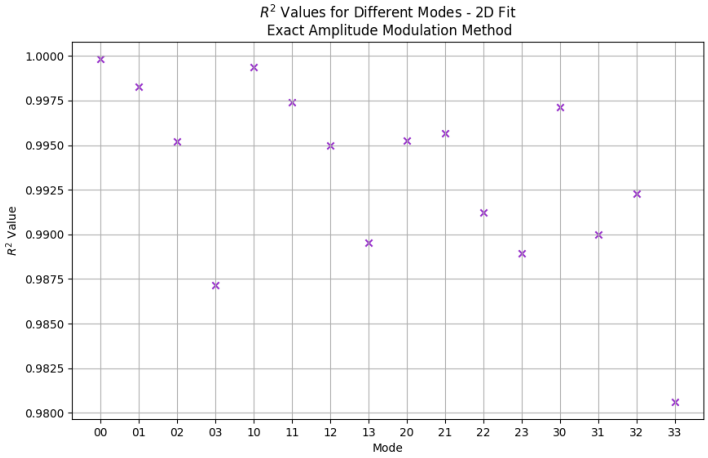

Figure 3.12: R^2 values for different LG modes using the exact amplitude modulation method.

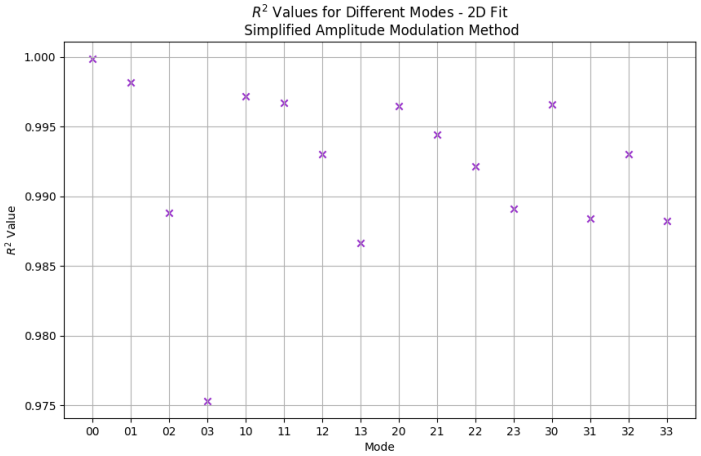

Figure 3.13: R^2 values for different LG modes using the simplified amplitude modulation method.

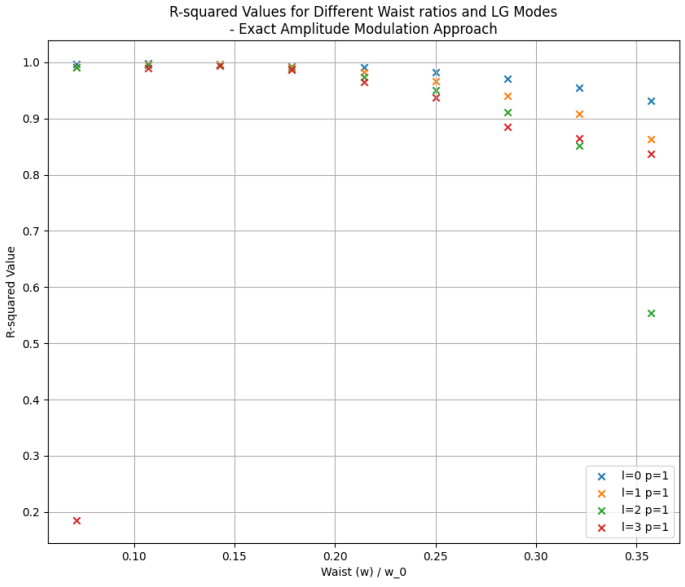

Figure 3.14: Mode purity for different LG modes using the exact amplitude modulation method.

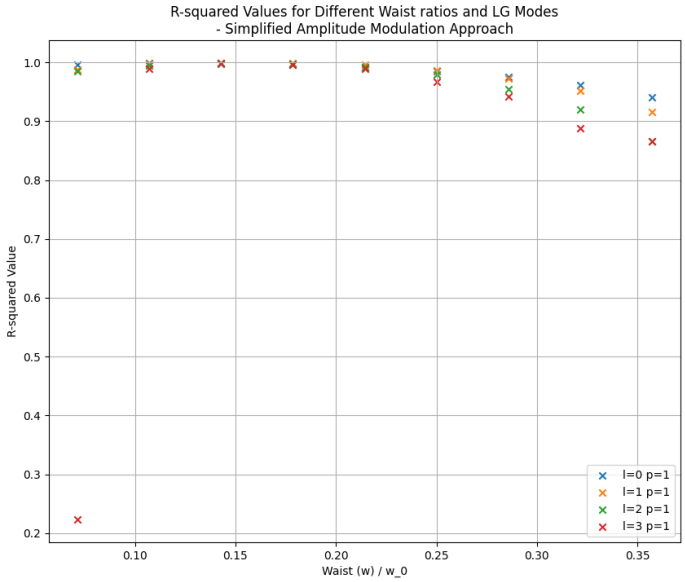

Figure 3.15: Mode purity for different LG modes using the simplified amplitude modulation method.

CHAPTER 4

Experimental Generation of Laguerre-Gaussian Modes

This chapter presents the experimental setup and methods used to generate Laguerre-Gaussian (LG) modes. Following the theoretical background and numerical simulations, the focus shifts to the practical implementation of these modes using a Spatial Light Modulator (SLM). The experimental setup is designed to accurately modulate the phase of an incoming laser beam to create the desired LG modes, while adjustments in the optical components ensure optimal beam quality. The results provide a comparison between simulated and experimentally generated modes, highlighting the practical challenges and achievements in the field.

4.1 Experimental Setup

The experimental setup used in this thesis is primarily based on the work done by Kimberly Kurzbach[7], with specific modifications to improve the imaging of the resulting modes. The light source is a 780 nm extended cavity diode laser[18], which is fiber-coupled to clean the beam shape and then reflected off a Liquid Crystal on Silicon Spatial Light Modulator (LCOS-SLM) before being focused onto a camera. A schematic of the setup is shown in Figure , and the key components are described below.

The laser is equipped with an optical isolator to protect it from back reflections that could potentially cause damage. Neutral density (ND) filters are used to adjust the intensity of the laser beam before it is coupled into a fiber, which avoids interference effects near the camera. A half-wave plate (HWP) is used to rotate the polarization of the beam, aligning it with the LC layer of the SLM. The polarization is further checked using a polarizing beam splitter (PBS), ensuring that almost 98% of the light is horizontally polarized before reaching the SLM.

The beam is then expanded using a telescope consisting of two lenses to match the size of the effective area of the SLM. This setup ensures the laser beam properly interacts with the SLM's surface to spatially modulate its phase according to the displayed holograms. An angle of incidence of $\theta \leq 5^{\circ}$ is maintained to minimize distortions, as larger angles would increase the effective pixel size and distort the resulting image.

After modulation by the SLM, the beam passes through a second telescope designed to perform a Fourier transformation of the modulated wavefront. This telescope, which consists of a convex and a concave lens, was modified in this work to achieve better magnification. The original second lens, with

a focal length of $f = -50\,\text{mm}$, was replaced by an $f = -100\,\text{mm}$ lens, increasing the image size on the camera. Due to this change, the lenses were positioned approximately 8 cm apart, and the resulting focal plane was calculated to be about 28 cm from the first lens using a Gaussian beam calculator. The camera was positioned at this location to accurately capture the Fourier-transformed image.

The camera used in this setup is the LaserCam HR II from Coherent, which offers a resolution of 1280×1024 pixels and a pixel size of $6.5 \times 6.5\,\mu\text{m}$, providing higher image quality than the previously used camera.[19]

For a more comprehensive understanding of the original setup, including detailed component specifications, readers are referred to the bachelor thesis of Kimberly Kurzbach[7].

4.2 Results from Laguerre-Gaussian Mode Generation

In this section, the results of experimentally generating Laguerre-Gaussian (LG) modes using the experimental setup described in Section 4.1 are presented. The experiments focused on generating LG modes with varying azimuthal (l) and radial (p) indices using both phase-only and amplitude-modulated holograms. The generated modes were captured by a high-resolution camera and analyzed to evaluate the accuracy of the mode generation compared to theoretical expectations and numerical simulations. The performance of each hologram type is assessed based on the fidelity of the generated modes, the intensity distribution, and the corresponding fit parameters, providing insights into the effectiveness of the holographic generation techniques in producing high-quality LG modes.

4.2.1 Phase-Only Method

Optimal Waist Determination

The optimal waist of the phase mask was experimentally determined by analyzing the R^2 values for various waist sizes of the Laguerre-Gaussian (LG) modes. Figure 4.1 shows that the best waist was found to be 65 pixels with an initial beam waist $w_0 = 280$, resulting in a ratio of approximately 0.23. This is notably different from the simulation results, where a smaller range was analyzed due to resolution limitations. This discrepancy highlights the impact of having a broader experimental range without resolution constraints.

Experimental Diffraction Patterns

The experimentally generated first-order diffraction patterns for various LG modes using the phase-only method are presented in Figure 4.2. While the modes are generally well-formed, they exhibit noticeable distortions and ring structures, which deviate from the theoretically predicted patterns. These imperfections suggest a discrepancy in mode purity and quality when compared to simulations.

Waist Measurements

Figure 4.3 illustrates the measured waists in the x and y directions for the generated LG modes. The data indicates a lack of symmetry between the x and y waists, which deviates significantly from the simulated results. The mean waist values are as follows:

- Mean w_x: $0.0005749\,\text{m}$, Variance $4.54 \times 10^{-9}\,\text{m}^2$

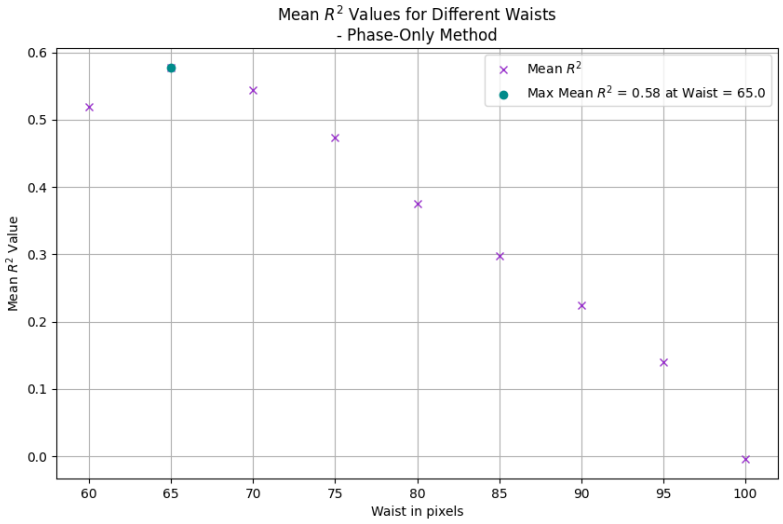

Figure 4.1: R^2 Values for Different Phasemask Waists - Phase-Only Mode. The optimal waist of 65 pixels corresponds to a ratio of approximately 0.23, which differs from the simulation results.

- Mean w_y: 0.0005292 m, Variance 4.31×10^{-9} m^2

The increased variance compared to simulation suggests potential alignment and setup inaccuracies.

R^2 Values for Experimental Modes

The R^2 values, which quantify the mode purity, are depicted in Figure 4.4. The average R^2 value is approximately 0.577, which is notably lower than the simulation results, highlighting the challenges in achieving high fidelity with phase-only holograms in an experimental setup.

Mode Purity Analysis

Figures 4.5 and 4.6 show the mode purity (quantified as R^2) for different LG modes and waist ratios. Consistent with simulation observations, the optimal waist shifts slightly for different modes, and a similar dependency on the waist ratio is observed. However, the experimental purity trends indicate greater variability, suggesting practical limitations such as optical alignment, phase distortions, and other experimental uncertainties.

4.2.2 Comparison of Amplitude Modulation Methods

The comparison between the simplified and exact amplitude modulation methods in the experimental setup shows notable differences and similarities to the simulations. Below, we summarize the key observations.

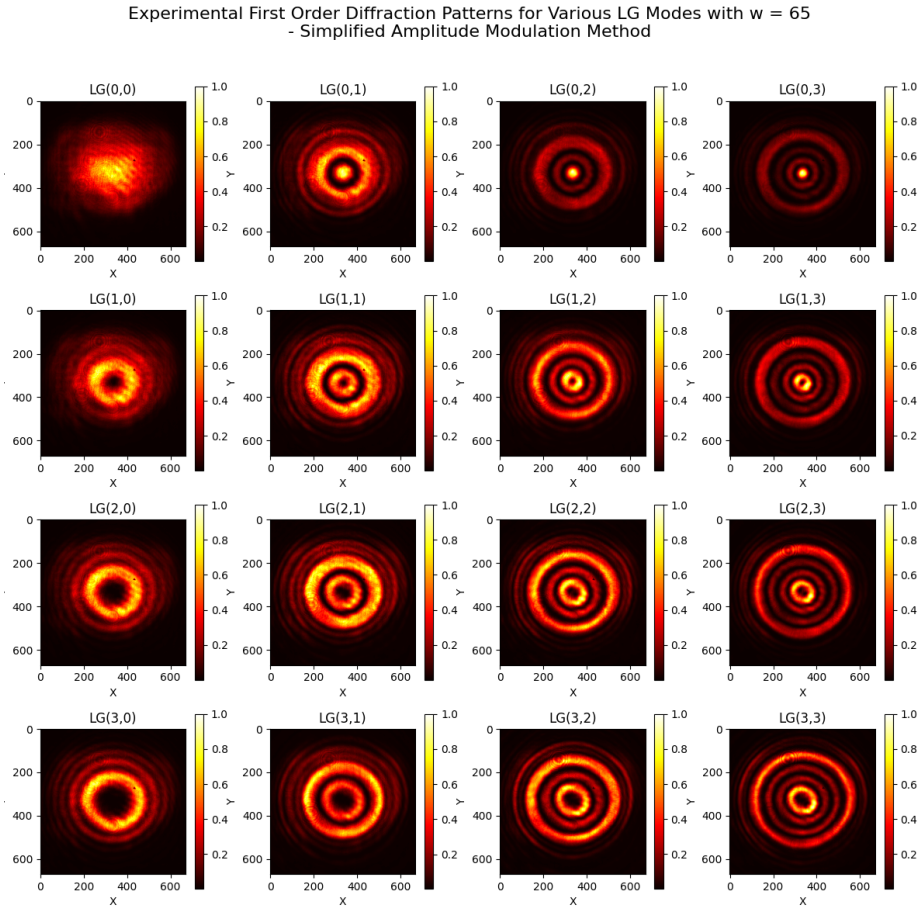

Figure 4.2: Experimental First Order Diffraction Patterns for Various LG Modes using Phase-Only Method. Distortions and ring structures are visible, indicating deviations from ideal mode formation.

Optimized Waist Values

Figures 4.7 and 4.8 display the dependency of R^2 values on different phasemask waists for both methods. In the simplified method, the best waist is found at $w = 45$ pixels, corresponding to a ratio of approximately 0.16 when $w_0 = 280$. For the exact method, the best waist is at $w = 50$ pixels, corresponding to a ratio of 0.18. These ratios differ from the simulation due to the broader range examined in the experimental setup.

Generated Modes

As shown in Figures 4.9 and 4.10, the generated Laguerre-Gaussian modes from both methods look visually consistent with the theoretical predictions, with no discernible differences between the methods.

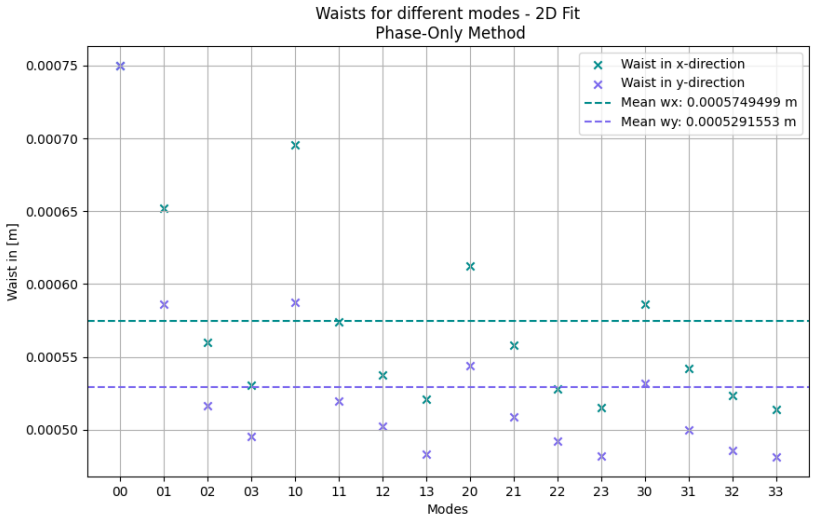

Figure 4.3: Waist Measurements for Different LG Modes - Phase-Only Method. Significant discrepancies between x and y waists are evident, indicating setup asymmetries.

Waist Discrepancy

The discrepancies between waists in the x and y directions are more prominent in the simplified method compared to the exact method, as shown in Figures 4.11 and 4.12. Overall, both methods exhibit larger discrepancies compared to simulations. For the simplified method:

Simplified method:

- Mean w_x: $0.0005537\,m$, Variance w_x: $2.87 \times 10^{-11}\,m^2$
- Mean w_y: $0.0005367\,m$, Variance w_y: $2.26 \times 10^{-11}\,m^2$

Exact method:

- Mean w_x: $0.0005329\,m$, Variance w_x: $4.97 \times 10^{-11}\,m^2$
- Mean w_y: $0.0005105\,m$, Variance w_y: $2.32 \times 10^{-11}\,m^2$

R-squared Values

The R^2 values across different modes are relatively consistent for both methods, with the simplified method slightly underperforming compared to the exact method. The mean R^2 for the simplified method is 0.8832, while for the exact method it is 0.9009, indicating a minor difference of about 0.2%, slightly higher than the 0.1% observed in simulations.

4.3 Discussion and Comparison with Simulation

The experimental results for the generation of Laguerre-Gaussian (LG) modes using phase-only and amplitude-modulated holograms reveal a range of observations that are both consistent with and

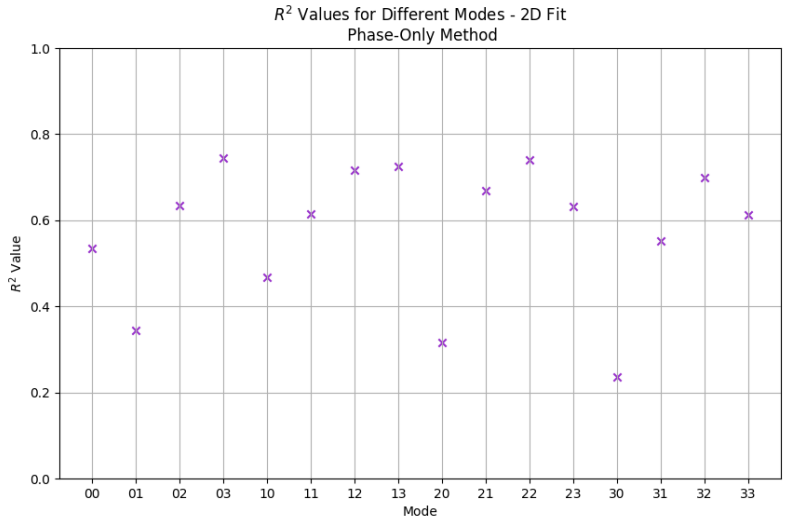

Figure 4.4: R^2 Values for Different Modes - Phase-Only Method. The average R^2 value of 0.577 is significantly lower than simulated values, indicating reduced mode purity.

divergent from the numerical simulations. This discussion critically evaluates the findings, identifies potential sources of discrepancies, and compares the fidelity of each method to the simulated results.

The determination of optimal waist values was a critical step in the generation process. For the phase-only method, the optimal waist was found to be 65 pixels with an initial beam waist $w_0 = 280$, resulting in a ratio of approximately 0.23. This ratio differs notably from the simulation results, where a smaller range was analyzed due to resolution limitations in the Fourier plane. This highlights the impact of broader experimental exploration, unencumbered by the numerical constraints faced in simulations. In the amplitude modulation methods, the optimized waists were found to be 45 pixels (ratio of 0.16) for the simplified method and 50 pixels (ratio of 0.18) for the exact method, both of which differ from simulated ratios. These differences can be attributed to the absence of the resolution constraints present in the experimental setup, allowing for a more comprehensive exploration of parameter space.

The generated diffraction patterns for both the phase-only and amplitude-modulated holograms exhibit high visual quality, with the LG modes appearing generally well-formed. However, closer inspection reveals specific deviations from ideal theoretical profiles. For the phase-only method, the generated patterns showed significant ring structures and distortions that were not as prominent in the simulations. These imperfections suggest that phase-only holograms may be more susceptible to aberrations in the optical system, such as misalignment, phase errors introduced by the SLM, and environmental instabilities. In contrast, both amplitude-modulated methods produced modes that closely resembled theoretical expectations, with minimal observable differences between the exact and simplified approaches. This indicates that amplitude modulation, especially in its exact form, offers improved resilience to such distortions, making it a preferable choice for high-fidelity mode generation.

Measurements of the waist sizes in the x and y directions revealed a notable lack of symmetry in the experimental setup, particularly for the phase-only method, where the discrepancy between w_x

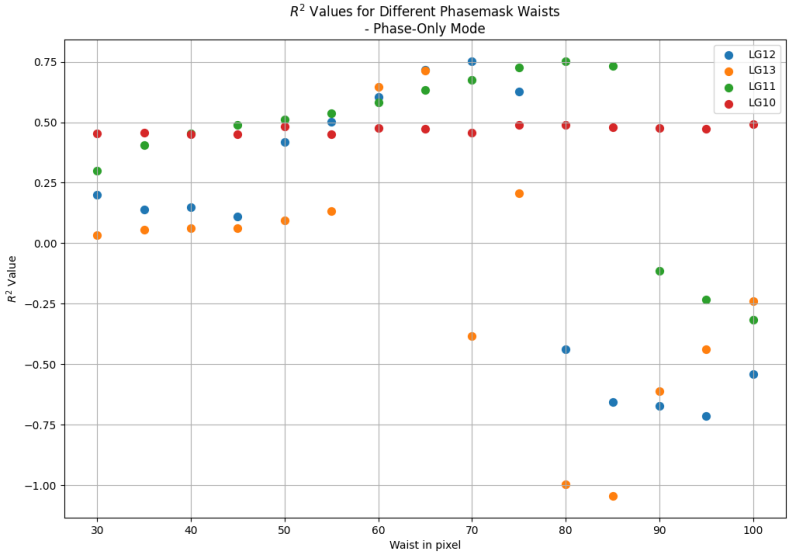

Figure 4.5: Mode Purity for Different l Values - Phase-Only Method. Variations in the optimal waist ratio for different modes are observed, reflecting similar dependencies seen in simulations.

and w_y was substantial. The variances in the measured waists were also higher than those observed in simulations, reflecting the compounded effects of optical misalignments and SLM performance inconsistencies. The amplitude modulation methods, particularly the exact approach, showed reduced discrepancies between x and y waists compared to the simplified method. This suggests that the exact amplitude modulation method maintains better control over mode symmetry, likely due to its more precise hologram generation process, which inherently reduces the influence of experimental imperfections.

The R^2 values provided a quantitative measure of the fidelity of the generated modes compared to theoretical profiles. For the phase-only method, the mean R^2 value was approximately 0.577, significantly lower than the values obtained in simulations, where R^2 was 0.68. This substantial drop in fidelity underscores the limitations of phase-only holograms in experimental conditions, highlighting potential sources of error such as limited phase modulation depth, imperfections in the SLM surface, and phase noise. In contrast, the amplitude modulation methods achieved mean R^2 values of 0.8832 for the simplified and 0.9009 for the exact approach. While these values are still below the near-perfect fidelity observed in simulations, they represent a marked improvement over the phase-only results. The slightly better performance of the exact method compared to the simplified approach suggests that the additional complexity of exact amplitude modulation pays off in terms of generating higher quality modes.

The mode purity analysis for the phase-only method revealed that the optimal waist shifted slightly for different LG modes, consistent with simulation trends, but with greater variability in experimental results. This variability points to the influence of practical limitations, such as optical misalignment, phase distortions, and noise, which were not fully captured in the simulations. Unfortunately, the mode purity data for the amplitude modulation methods were lost, preventing a direct comparison.

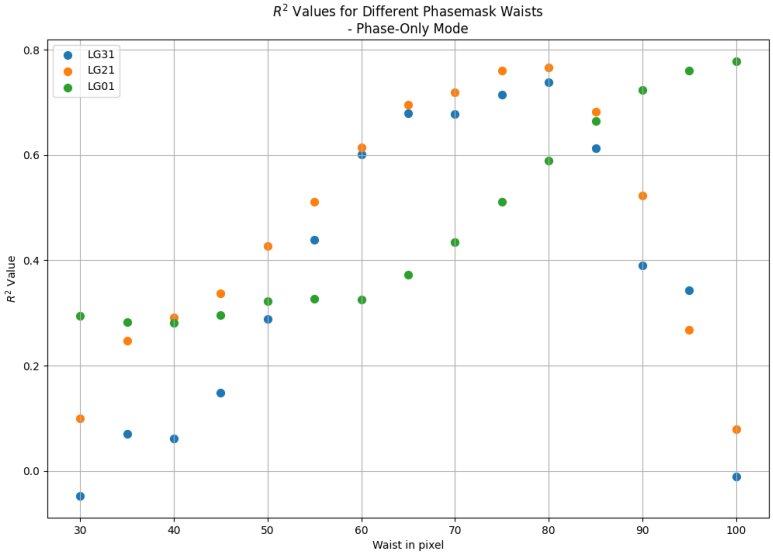

Figure 4.6: Mode Purity for Different p Values - Phase-Only Method. A similar trend of mode purity variation as a function of waist ratio is seen, albeit with greater experimental variability.

However, based on the consistent trends observed in simulations, it can be reasonably inferred that both amplitude methods would show similar dependencies on waist ratios, with the exact method likely maintaining slightly higher purity due to its more precise modulation capabilities.

Overall, the experimental findings validate the simulations to a significant extent, confirming that amplitude-modulated holograms, especially the exact approach, are highly effective for generating Laguerre-Gaussian modes with high fidelity. The observed discrepancies between experimental and simulated results underscore the importance of accounting for real-world imperfections when designing and optimizing optical systems for mode generation. Sources of experimental error include SLM imperfections, alignment inaccuracies, limited resolution of detection equipment, and environmental fluctuations, all of which contribute to deviations from the idealized conditions assumed in simulations. These insights are crucial for future refinements in experimental designs and underscore the need for robust calibration and alignment procedures to minimize the impact of these error sources.

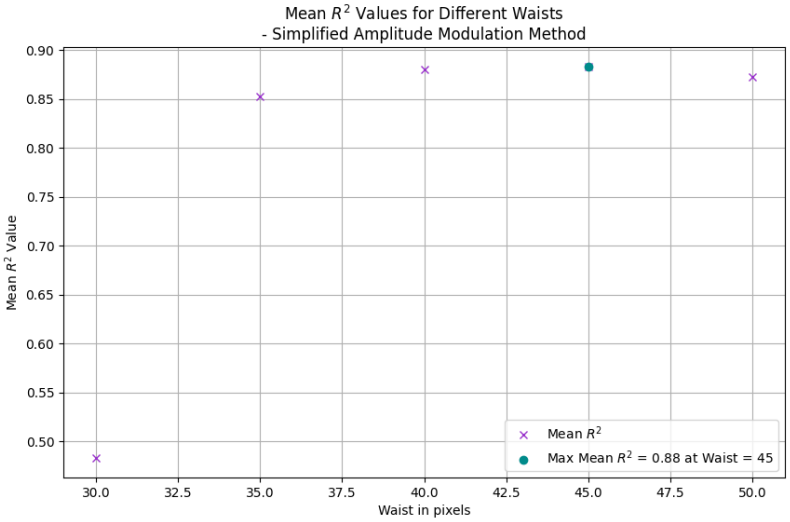

Figure 4.7: Mean R^2 values for different waists in the simplified amplitude modulation method. The optimal waist is at 45 pixels.

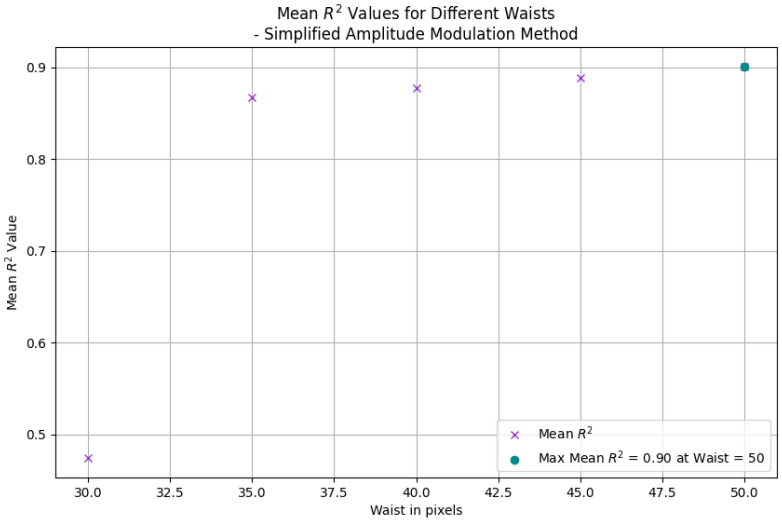

Figure 4.8: Mean R^2 values for different waists in the exact amplitude modulation method. The optimal waist is at 50 pixels.

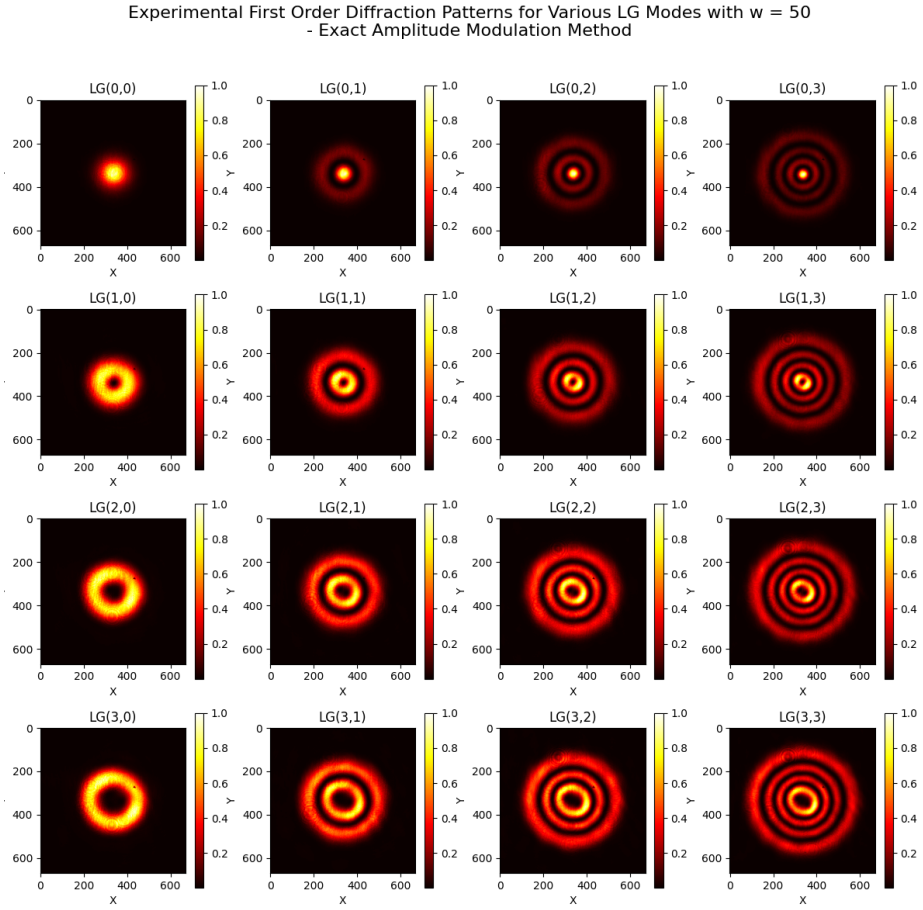

Figure 4.9: Experimental first-order diffraction patterns of various LG modes using the exact amplitude modulation method with optimized waist $w = 50$ pixels.

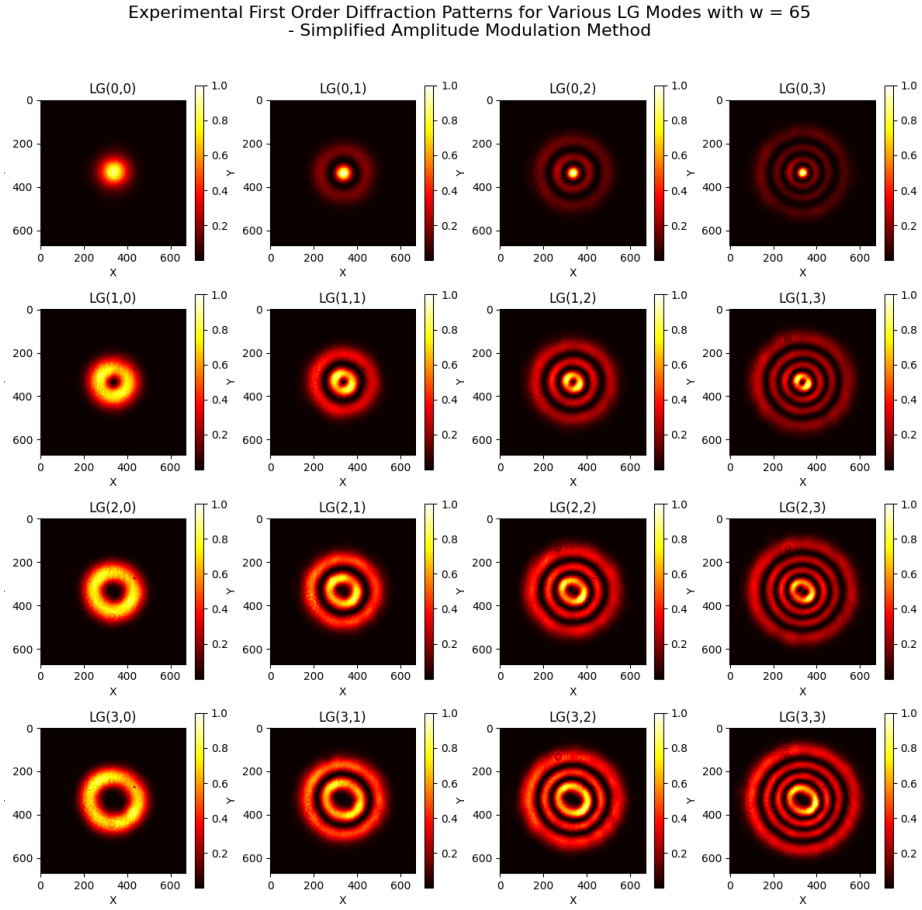

Figure 4.10: Experimental first-order diffraction patterns of various LG modes using the simplified amplitude modulation method with optimized waist $w = 45$ pixels.

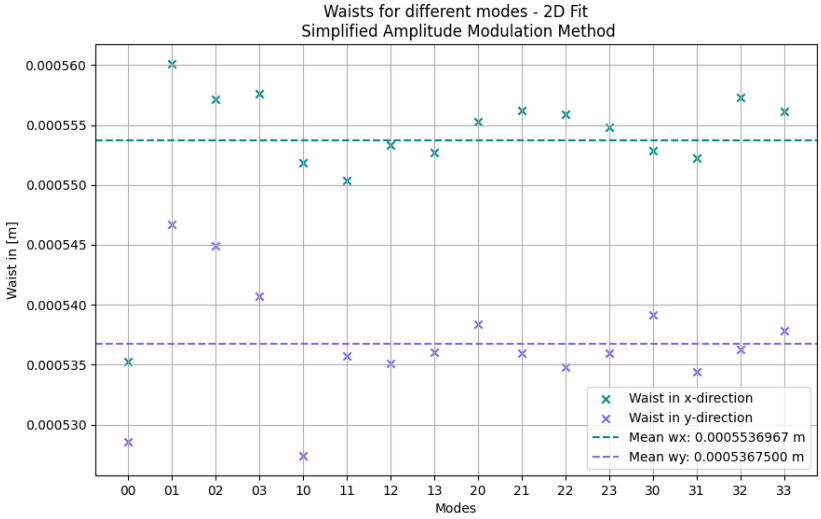

Figure 4.11: Measured waists in the x and y directions for different modes using the simplified amplitude modulation method.

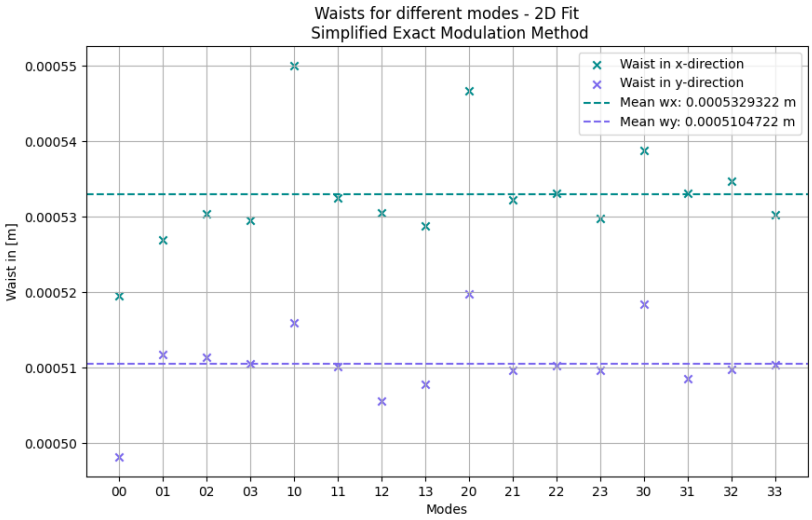

Figure 4.12: Measured waists in the x and y directions for different modes using the exact amplitude modulation method.

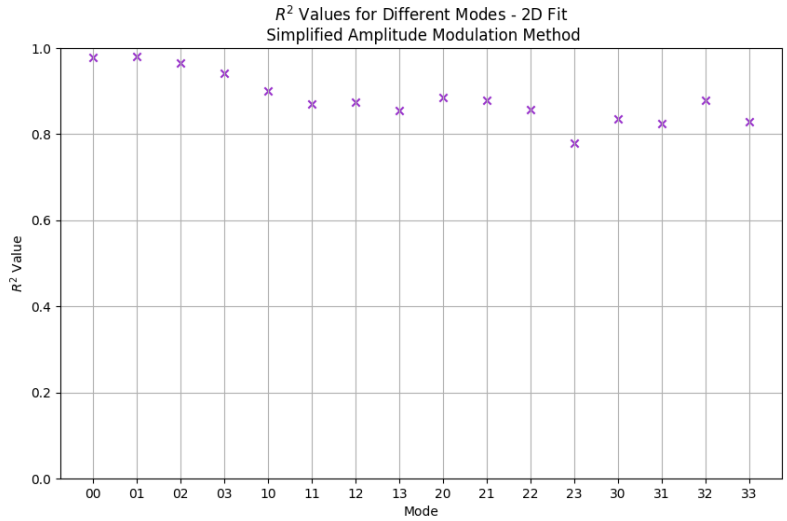

Figure 4.13: R^2 values for different modes using the simplified amplitude modulation method.

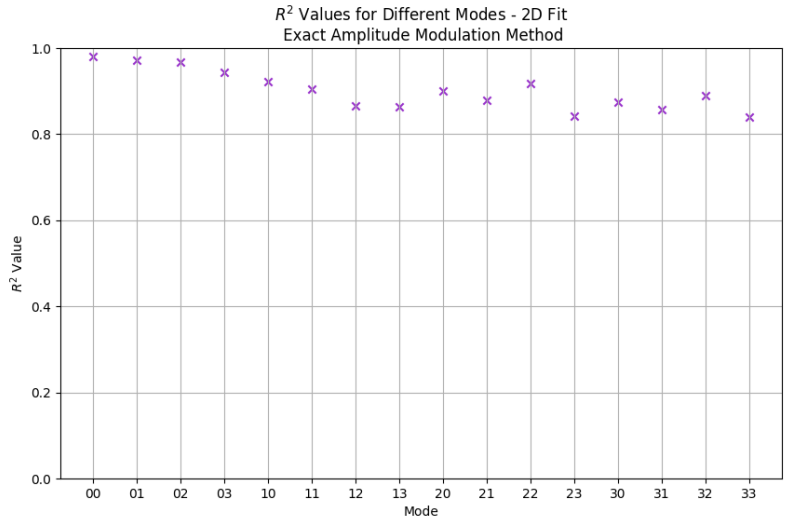

Figure 4.14: R^2 values for different modes using the exact amplitude modulation method.

CHAPTER 5

Conclusion and Outlook

This thesis presented a comprehensive study on the generation of Laguerre-Gaussian (LG) modes using phase-only and amplitude-modulated holograms, both theoretically and experimentally. The phase-only method and two variations of amplitude modulation—simplified and exact—were employed to generate LG modes, and their performance was evaluated through a combination of simulations and experimental measurements. The key findings of this research highlight the strengths and limitations of each approach, with a particular focus on mode purity, symmetry, and overall fidelity.

The experimental results for the phase-only method revealed that while it is capable of generating LG modes, the method suffers from significant distortions and variability in waist measurements compared to the simulations. The observed ring structures and reduced R^2 values suggest that phase-only holograms are more vulnerable to optical aberrations and setup imperfections. This highlights the need for careful alignment and calibration when using phase-only techniques in practical applications.

In contrast, the amplitude-modulated methods demonstrated superior performance, with the exact amplitude modulation approach achieving the highest fidelity and consistency. The exact method maintained better control over mode symmetry and purity, with R^2 values close to those observed in simulations. This indicates that the additional complexity of exact amplitude modulation is justified for applications requiring high-quality mode generation. The simplified amplitude modulation method, while slightly less accurate, still provided reliable results and offers a viable alternative when ease of implementation and computational efficiency are prioritized.

The overall comparison between experimental and simulated data underscores the importance of accounting for real-world imperfections such as SLM performance, alignment errors, and environmental factors, which can significantly impact mode generation. These insights are crucial for refining experimental designs and optimizing optical systems for future research and applications.

Looking ahead, there are several promising directions for further investigation. One potential area of improvement involves enhancing the stability and calibration of the optical setup, particularly for phase-only methods, to reduce alignment-induced errors and increase overall mode fidelity. Additionally, exploring advanced SLM technologies with improved phase modulation capabilities could help mitigate some of the performance limitations observed in the current study.

Further research could also extend the analysis to higher-order LG modes and other complex beam shapes, allowing for a deeper understanding of the generation techniques and their limitations. In the context of quantum optics, where precise control of light modes is critical, these advancements could

facilitate more sophisticated experiments, such as the manipulation of photons with orbital angular momentum in quantum communication and computation systems.

The integration of machine learning algorithms for real-time optimization and error correction in mode generation presents another exciting opportunity. Such approaches could dynamically adjust the hologram parameters to compensate for experimental imperfections, thereby enhancing the robustness and adaptability of the mode generation process.

In summary, this work lays the groundwork for further development of holographic techniques in generating high-quality optical modes. The insights gained here will be valuable not only for fundamental research in optical physics but also for practical applications in fields such as quantum optics, optical communication, and laser beam shaping.

Bibliography

[1] Yudong Lian, Xuan Qi, Yuhe Wang, Zhenxu Bai, Yulei Wang and Zhiwei Lu. **?**OAM beam generation in space and its applications: A review**? in***Optics and Lasers in Engineering*: 151 (2022), **pages** 1–17.

[2] S. Franke-Arnold. **?**Optical angular momentum and atoms**? in***Philosophical Transactions of the Royal Society A: Mathematical, Physical and Engineering Sciences*: 375.2087 (2017).

[3] O. Firstenberg, C. S. Adams **and** S. Hofferberth. **?**Nonlinear quantum optics mediated by Rydberg interactions**? in***Journal of Physics B: Atomic, Molecular and Optical Physics*: 49 (2016), **page** 152003. DOI: 10.1088/0953-4075/49/15/152003. URL: https://dx.doi.org/10.1088/0953-4075/49/15/152003.

[4] J. Kumlin **andothers**. **?**Quantum Optics with Rydberg Superatoms**? in***Journal of Physics Communications*: (2023).

[5] Thomas W. Clark, Rachel F. Offer, Sonja Franke-Arnold, Aidan S. Arnold and Neal Radwell. **?**Comparison of beam generation techniques using a phase-only spatial light modulator**? in***Journal of the Optical Society of America A*: 24.6 (2016), **pages** 6249–6264. URL: https://opg.optica.org/josaa/abstract.cfm?uri=josaa-33-7-1328.

[6] A. Ya. Bekshaev, S. V. Sviridova, A. Yu. Popov and A. V. Tyurin. **?**Generation of Optical Vortex Light Beams by Volume Holograms with Embedded Phase Singularity**? in** *I.I. Mechnikov National University*: (2024).

[7] K. Kurzbach. **?**Generation and Detection of Optical Beams with Orbital Angular Momentum using a Spatial Light Modulator**?** Bachelor Thesis. Bonn, Germany: University of Bonn, May 2024.

[8] Naoya Matsumoto, Taro Ando, Takashi Inoue, Yoshiyuki Ohtake, Norihiro Fukuchi and Tsutomu Hara. **?**Generation of high-quality higher-order Laguerre–Gaussian beams using liquid-crystal-on-silicon spatial light modulators**? in***Journal of the Optical Society of America A*: 25.7 (2008), **pages** 1642–1651. URL: https://opg.optica.org/josaa/abstract.cfm?uri=josaa-25-7-1642.

[9] Yoshiyuki Ohtake, Taro Ando, Norihiro Fukuchi, Naoya Matsumoto, Haruyasu Ito and Tsutomu Hara. **?**Universal generation of higher-order multiringed Laguerre–Gaussian beams by using a spatial light modulator**? in***Optics Letters*: 32.11 (2007), **pages** 1411–1412. URL: https://opg.optica.org/josaa/abstract.cfm?uri=josaa-24-5-1083.

[10] Eliot Bolduc, Nicolas Bent, Enrico Santamato, Ebrahim Karimi and Robert W. Boyd. **?**Exact solution to simultaneous intensity and phase encryption with a single phase-only hologram**?** **in***Optics Letters*: 38.18 (2013), **pages** 3546–3549. URL: http://dx.doi.org/10.1364/OL.38.003546.

[11] Jeffrey A. Davis, Don M. Cottrell, Juan Campos, María J. Yzuel and Ignacio Moreno. **?**Encoding amplitude information onto phase-only filters**?** **in***Applied Optics*: 38.23 (1999), **pages** 5004–5013.

[12] J. W. Goodman. *Introduction to Fourier Optics*. 2nd. McGraw-Hill, Inc., 1996.

[13] C. A. Bennett. *Principles of Physical Optics*. New Jersey: John Wiley & Sons, Inc., 2008.

[14] A. K. Ersoy. *Diffraction, Fourier Optics and Imaging*. New Jersey: John Wiley & Sons, Inc., 2007.

[15] Hamamatsu. *LCOS-SLM Software Operation Manual*. D. Hamamatsu Photonics K.K. 2016.

[16] G. Dijk. **?**Intensity patterns generated with a Spatial Light Modulator**?** Master's thesis. Eindhoven University of Technology, 2012.

[17] J. A. de Haan. *Holographic Generation of Arbitrary Intensity Patterns*. Bachelor's thesis. 2022.

[18] Vitawave. *Technical description and instruction manual of an extended cavity diode laser ECDL-7830R (S/N 121111)*. Accessed: 2024-09-02. n.d. URL: https://wiki.nqo.uni-bonn.de/images/ECDL-7830R_121111_Vitaly.pdf.

[19] Coherent Inc. *LaserCam-HR II High-Resolution Laser Beam Profiling System Manual*. Technical description and instruction manual. n.d.

Acknowledgments

I would like to express my deepest gratitude to the entire NQO group for being such a lovely, welcoming, and supportive community. Your kindness and camaraderie made my time here incredibly rewarding.

A special thank you goes to Daniil and Nina for always being ready to help me with my countless questions, and to everyone else in the lab who supported me along the way. I am genuinely grateful to have had the opportunity to write my bachelor thesis in this incredible group.

I would also like to thank Professor Dr. Sebastian Hofferberth for allowing me to pursue my bachelor thesis under his guidance. Additionally, my heartfelt thanks go to Prof. Dr. Daqing Wang for agreeing to be my second examiner.

Lastly, I want to express my deepest appreciation to my family, friends, and everyone who supported and encouraged me throughout this journey. Your unwavering belief in me helped me ace this thesis. Thank you all from the bottom of my heart.